

Collapse mechanism maps for a hollow pyramidal lattice

S. M. Pingle, N. A. Fleck, V. S. Deshpande and H. N. G. Wadley

Proc. R. Soc. A published online 13 October 2010

doi: 10.1098/rspa.2010.0329

Supplementary data

["Data Supplement"](#)

<http://rspa.royalsocietypublishing.org/content/suppl/2010/10/13/rspa.2010.0329.DC1.html>

References

[This article cites 25 articles, 2 of which can be accessed free](#)

<http://rspa.royalsocietypublishing.org/content/early/2010/10/13/rspa.2010.0329.full.html#ref-list-1>

P<P

Published online 13 October 2010 in advance of the print journal.

Subject collections

Articles on similar topics can be found in the following collections

[materials science](#) (151 articles)
[mechanical engineering](#) (145 articles)
[structural engineering](#) (32 articles)

Email alerting service

Receive free email alerts when new articles cite this article - sign up in the box at the top right-hand corner of the article or click [here](#)

Advance online articles have been peer reviewed and accepted for publication but have not yet appeared in the paper journal (edited, typeset versions may be posted when available prior to final publication). Advance online articles are citable and establish publication priority; they are indexed by PubMed from initial publication. Citations to Advance online articles must include the digital object identifier (DOIs) and date of initial publication.

To subscribe to *Proc. R. Soc. A* go to: <http://rspa.royalsocietypublishing.org/subscriptions>

Collapse mechanism maps for a hollow pyramidal lattice

BY S. M. PINGLE¹, N. A. FLECK^{1,*}, V. S. DESHPANDE¹
AND H. N. G. WADLEY²

¹*Department of Engineering, University of Cambridge, Trumpington Street, Cambridge CB2 1PZ, UK*

²*Department of Materials Science and Engineering, University of Virginia, Wilsdorf Hall, PO Box 400745, Charlottesville, VA 22904, USA*

Cellular materials with hollow lattice truss topologies exhibit higher compressive strengths than equivalent structures with solid trusses owing to their greater resistance to plastic buckling. Consequently, hollow trusses have attracted interest as the cores for sandwich panels. Finite-element calculations are used to investigate the elastic–plastic compressive collapse of a metallic sandwich core made from vertical or inclined circular tubes, made from annealed AISI 304 stainless steel. First, the dependence of the axial compressive collapse mode upon tube geometry is determined for vertical tubes with built-in ends and is displayed in the form of a collapse mechanism map. Second, the approach is extended to inclined circular hollow tubes arranged as a pyramidal lattice core; the collapse modes are identified and the peak compressive strength is determined as a function of geometry. For a given relative density of hollow pyramidal core, the inclined tube geometry that maximizes peak strength is identified. The predicted collapse modes and loads for the pyramidal core are in excellent agreement with measurements for the limited set of experimentally investigated geometries.

Keywords: lattice materials; sandwich structures; finite-element analysis; collapse mechanism maps

1. Introduction

Sandwich panels typically comprise two face sheets of high in-plane stiffness and strength separated by a low-density core (Zenkert 1995). The primary function of the core is to increase the structural bending stiffness by separation of the face sheets, and to carry transverse shear and compressive loads. The pyramidal lattice core is advantageous as it possesses a high shear strength at low relative density $\bar{\rho}$, as defined by the ratio of density of the cellular solid to that of the solid material (Deshpande & Fleck 2001). In some applications, such as impact or impulsive load mitigation, the sandwich is subjected to significant through-thickness compressive loading (Fleck & Deshpande 2004) and the pyramidal

*Author for correspondence (nafl@eng.cam.ac.uk).

Electronic supplementary material is available at <http://dx.doi.org/10.1098/rspa.2010.0329> or via <http://rspa.royalsocietypublishing.org>.

core is compromised by plastic buckling. The recent tests by Queheillalt & Wadley (submitted) reveal that a pyramidal core made from hollow struts has a substantially higher compressive strength than a pyramidal core made from solid struts. This motivates the present paper: the challenge is to determine the collapse modes and associated compressive strengths for a pyramidal core made from both hollow struts and solid struts. Additionally, the collapse response of a sandwich core made from vertical hollow tubes is obtained, for comparison.

The practical interest in sandwich panels with lattice cores has been heightened by recent innovations in manufacturing (Wadley 2006). Cellular materials achieve a low relative density $\bar{\rho}$ by gas-bubble generation, the incorporation of hollow particles or the use of sacrificial space holders to produce foam or by the assembly and the bonding of plates or trusses to create lattice materials.

Cellular materials find application as the cores of sandwich panels in part because they are able to convert the kinetic energy of an impact event to plastic deformation within the core. The most commonly used impact mitigation materials are foams that are manufactured mostly from the melt by the expansion of gas bubbles. The expansion process is thermodynamically driven by the minimization of internal pressure and surface energy. Since the gas-generating particles are randomly dispersed, this leads to stochastic topology foam with a low nodal connectivity of three to four for adjoining cell edges. The small nodal connectivity leads to a stiffness and strength of these three-dimensional structures that is governed by the bending stiffness of the cell edges and foams are consequently referred to as *bending-dominated structures*. The elastic modulus and strength then scale as $\bar{\rho}^2$ and $\bar{\rho}^{3/2}$, respectively (Deshpande *et al.* 2001*b*). In contrast, lattice materials are periodic, micro-architected cellular solids in which the individual elements can be oriented to deform by stretching rather than by bending (figure 1). Consequently, both the stiffness and strength of lattice materials scale linearly with their relative density and they compete favourably with foams as the cores of sandwich panels (Ashby *et al.* 2000; Deshpande *et al.* 2001*b*).

Lattice topologies can be classified as prismatic, honeycomb or truss based, as summarized in figure 1. Triangular and diamond corrugations and the Navtruss structures are examples of prismatic lattice materials. Honeycombs are closed cell structures made of webs that are perpendicular to the faces. These webs can be arranged to form triangular, square or hexagonal cells. Lattice truss structures are assembled from inclined struts of arbitrary cross section (square, round, etc). Examples include the tetrahedral, pyramidal and Kagome lattice truss topologies in which either three, four or six trusses meet at a node. In addition to high stiffness and strength, truss-based lattice structures are well suited to multi-functional applications such as cross-flow heat exchange owing to their open interior structure (Tian *et al.* 2006; Queheillalt *et al.* 2008). The superiority of the thermo-structural characteristics of a periodic truss core is confirmed by Evans *et al.* (1998, 2001), Deshpande *et al.* (2001*a,b*) and Wicks & Hutchinson (2001).

It is emphasized at this point that a degree of confusion has entered the literature with regard to the use of the word ‘truss’. In the structural mechanics literature, the term truss usually refers to a pin-jointed strut, whereas in the materials literature it can also refer to a rigidly jointed member. In the present study, we shall consider a lattice core that is rigidly welded to the face sheets so that the ends of the struts are fully constrained against relative motion (rotation

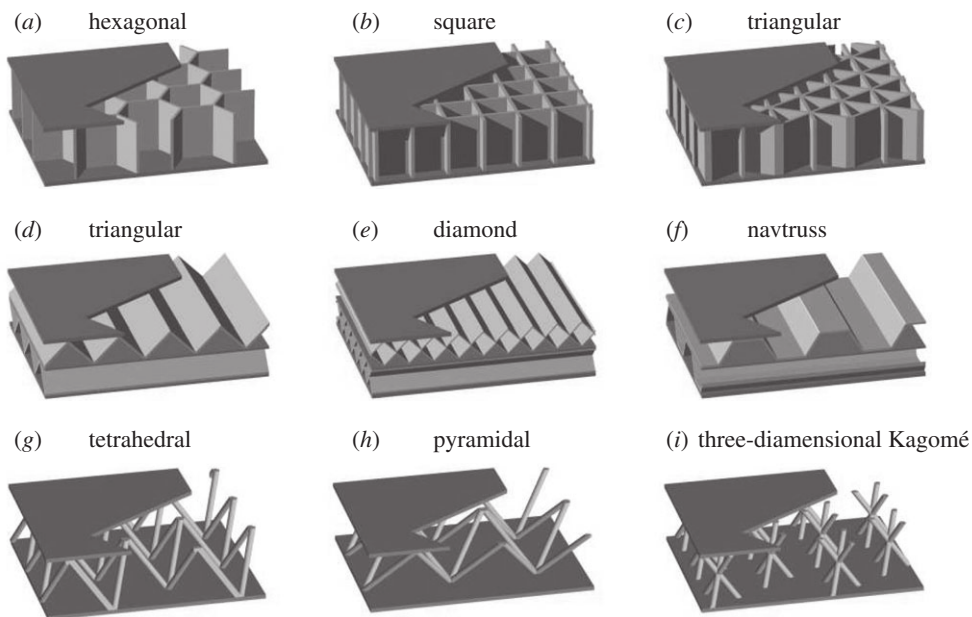


Figure 1. Examples of lattice materials. (a)–(c) are honeycombs, (d)–(f) are prismatic and (g)–(i) are truss based.

and displacement). We shall refer to such a core as a pyramidal truss, to follow the materials convention, although it would be more precise to refer to the lattice by the lengthier descriptor of ‘rigidly jointed framework’.

The dependence of compressive strength upon relative density for lattice materials and foams is contrasted with that for fully dense engineering solids in figure 2*a*. Lattice materials fill a large portion of material property space, but there is scope for future improvements in topological design to generate materials that lay in the region labelled ‘future materials’.

Figure 2*a* shows three lines emanating from the titanium ‘bubble’. These correspond to the predicted strengths of a titanium diamond corrugation, a square honeycomb and a pyramidal lattice with solid struts. As the relative density of periodic cellular solids is reduced, in each case, the compressive strength becomes dominated by web or truss buckling, and the strength drops steeply with any further reduction in relative density. This transition in response from plastic collapse to elastic buckling occurs at very low relative densities (below 1%) for the truss-based lattice structures, and at a higher relative density on the order of 10 per cent for honeycombs. Additional stabilization against buckling is obtained by increasing the second moment of area through use of hollow struts (Timoshenko & Gere 1961) and this effect is addressed in the present paper. Recent experiments have demonstrated that hollow truss cores with diamond and square orientations made from stainless steels offer significant structural advantage over their solid truss counterparts, see figure 2*b* and Queheillalt & Wadley (2005*a,b*, submitted). In figure 2*b*, the measured peak strength σ_{pk} has been normalized by the relative density $\bar{\rho}$ and yield strength $\sigma_Y = 180$ MPa of the stainless steel in order to illustrate the structural efficiency of the hollow trusses. When buckling modes

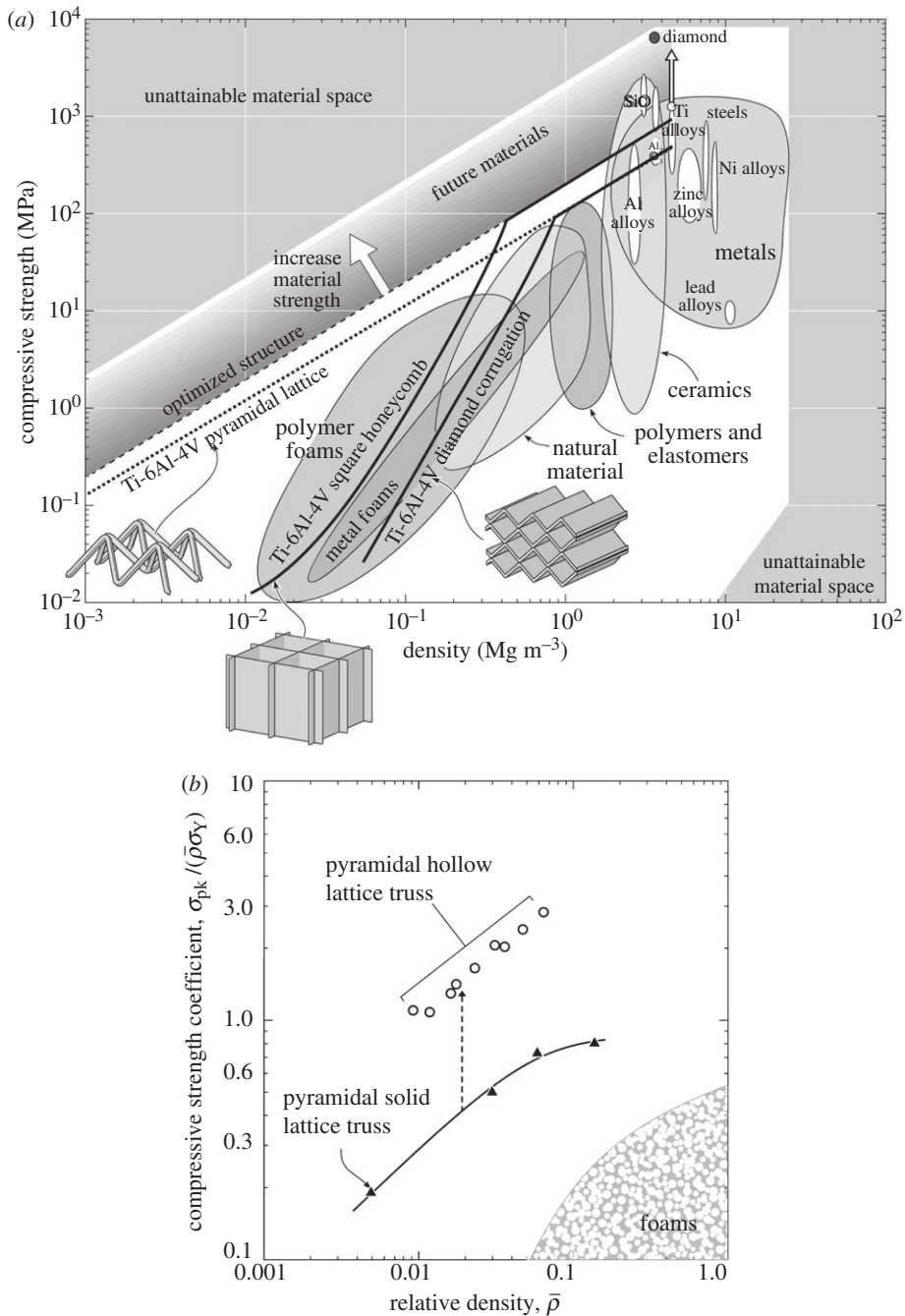


Figure 2. (a) The compressive strength of lattice materials shown on a plot of strength versus density along with other engineering materials. (b) The normalized compressive peak strength of 304 stainless steel hollow pyramidal lattice structures compared with equivalent pyramidal cores made from solid struts and metal foams. Adapted in modified form from Queheillalt & Wadley (submitted).

are suppressed, there is an opportunity to extend the ‘truss structures’ line on figure 2*a* to lower densities (denoted by the dashed extension of the titanium pyramidal lattice line). An increase in the strength of the material used to make these optimized trusses then opens up an opportunity identified as ‘future materials’ in figure 2*a*.

There are, however, manufacturing challenges associated with sandwich cores made from hollow trusses (Kooistra & Wadley 2007):

- The limited bonded area between the core and face sheets may lead to debonding;
- The conventional manufacturing method (of node row folding) used to make lattice truss structures is difficult to implement for hollow trusses (Queheillalt & Wadley 2005*a,b*).

Queheillalt & Wadley (submitted) have proposed a tube insertion method for tackling both shortcomings. This method ensured efficient material usage and a robust node design. Sandwich structures with hollow pyramidal core ($\bar{\rho} = 0.9\text{--}5.8\%$) made from annealed AISI type 304 stainless steel were fabricated in this manner, and their through-thickness compressive and transverse shear strengths were measured (Queheillalt & Wadley submitted). They found that the compressive strength and energy absorption of these cores were 1.5–2 times that of the equivalent solid truss, depending upon the stockiness and wall thickness of the tubular core.

The compressive strength of the core depends upon the length l , outer diameter d and wall thickness t of the tubes, as defined in figure 3*a*. The slenderness ratio is given by l/d , and the normalized wall thickness is t/d . The collapse modes observed by Queheillalt & Wadley (submitted) are shown in table 1, for two selected values of l/d and t/d . The thick-walled, stocky struts underwent plastic collapse without buckling, whereas the more slender, thinner walled struts buckled plastically or elastically. We note in passing that the yield strain of the cell wall material also plays a role: a material of high yield strain is more likely to buckle elastically than plastically.

(*a*) Review of the axial compressive collapse of ductile circular tubes

A literature on the elasto-plastic axial collapse of circular tubes predates the literature on lattice materials made from hollow struts. Since the collapse modes are closely related, it is instructive to review existing knowledge on the axial collapse of a circular tube. This has been studied from two perspectives:

- As a bifurcation problem to rigorously define the transition from elastic to inelastic buckling and to investigate the significance of geometric imperfections (e.g. Brush & Almroth 1975).
- As a large-strain elasto-plastic collapse problem focusing on energy absorption during collapse (Johnson & Reid 1978; Abramowicz & Jones 1997).

This second approach is motivated by the use of thin-walled tube sections as primary impact energy-absorbing structural members in land, marine and aerospace transportation systems because of their high structural efficiency

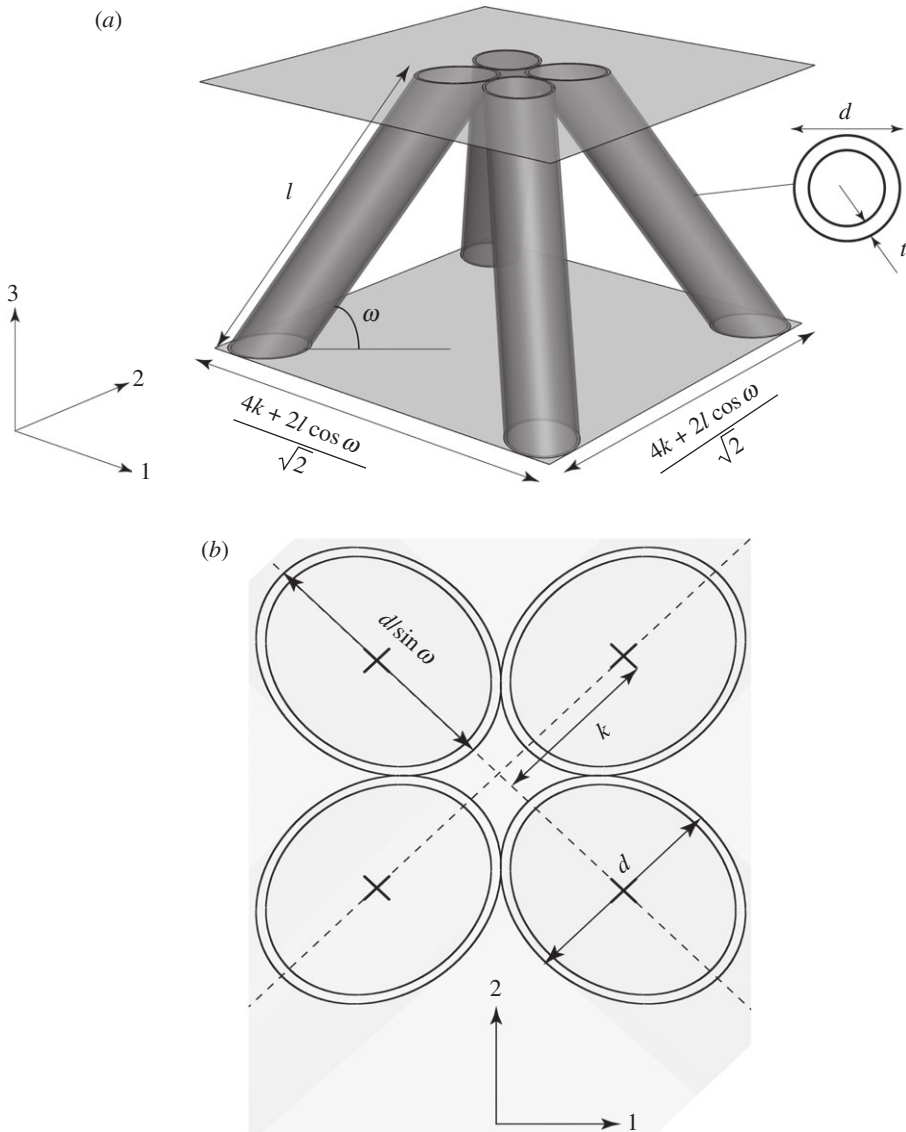

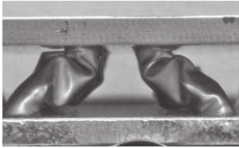

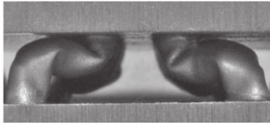


Figure 3. (a) Unit cell of the hollow pyramidal core with the four struts touching at the top surface. (b) Plan view of the four hollow struts on a plane corresponding to the lower surface of the top face sheet. The separation between tubes equals $2k$, and adjacent tubes touch when $k = k_{\min}$.

and low manufacturing cost. Circular tubes subjected to axial compression are effective for the plastic dissipation of impact energy over a long stroke distance (Johnson & Reid 1978).

The performance of thin-walled tubes as energy absorbers is governed by their collapse mode: the most desirable mode is by progressive axisymmetric folding. In well-designed tubes that collapse in this manner, a large fraction of the tube wall undergoes large plastic strain without significant fluctuations in axial load. The shell nature of the tube ensures that the tube wall is loaded biaxially during

Table 1. Comparison of the predicted and observed collapse modes of the hollow pyramidal lattice core. The comparison is shown for an applied compressive strain $\varepsilon_n = 0.5$. The observations are taken from the experimental study of Queheillalt & Wadley (submitted).

geometry	finite element prediction	experiment
exp. I $\frac{t}{d} = 0.04,$ $\frac{l}{d} = 4.88$		 mode C
exp. II $\frac{t}{d} = 0.08,$ $\frac{l}{d} = 4.88$		 mode E

collapse by a combination of stretching and bending. In contrast, a solid-walled column of the same length and mass as that of the hollow tube (but of much smaller diameter) absorbs less energy in axial collapse: a small number of plastic hinges (typically 1 or 2) are triggered in the solid-walled column and these engage only a small volume fraction of the material in plastic deformation.

The quasi-static, elasto-plastic axial collapse of a circular tube, of geometry shown in figure 4*a*, is a classical problem in solid mechanics. However, most previous studies have focused on a single collapse mechanism and a full classification of the collapse mechanisms as a function of tube geometry has not been addressed. Initial attempts to do so have been experimental in nature, as follows. Andrews *et al.* (1983) investigated the collapse modes and energy absorption properties of quasi-statically compressed aluminium alloy tubes. They identified several modes of buckling and mapped the regimes of dominance on a collapse mechanism map that is redrawn in figure 5*a*. The tubes were made from annealed Ht-30 aluminium alloy (of composition Cu 0.1%, Mg 0.4–1.5%, Si 0.6–1.3%, Fe 0.6%, Mn 0.4–1.0%, Zn 0.1%, Cr 0.5% and remainder Al); this alloy exhibits appreciable strain hardening as shown in figure 4*b*. Likewise, Guillow *et al.* (2001) have developed a collapse classification map (figure 5*b*) for tubes made from 6060-T5 aluminium alloy. In this heat-treated state, the 6060 aluminium alloy has a much higher strength (and yield strain) but displays negligible strain hardening (figure 4*b*). A comparison of the maps shown in figure 5*a,b* indicates that the differences in yield strain and in strain-hardening behaviours of the two alloys significantly affect the buckling modes and their regimes of dominance. For example, the regime of multiple folds is located at higher ratios of tube wall thickness to outer diameter (t/d) for the Ht-30 alloy than for the 6060-T5 alloy.

Abramowicz & Jones (1997) have experimentally investigated the static axial crushing of thin-walled *mild steel* tubes of square and circular cross sections. The steel was in the cold-worked condition, with a yield strength of 250–450 MPa

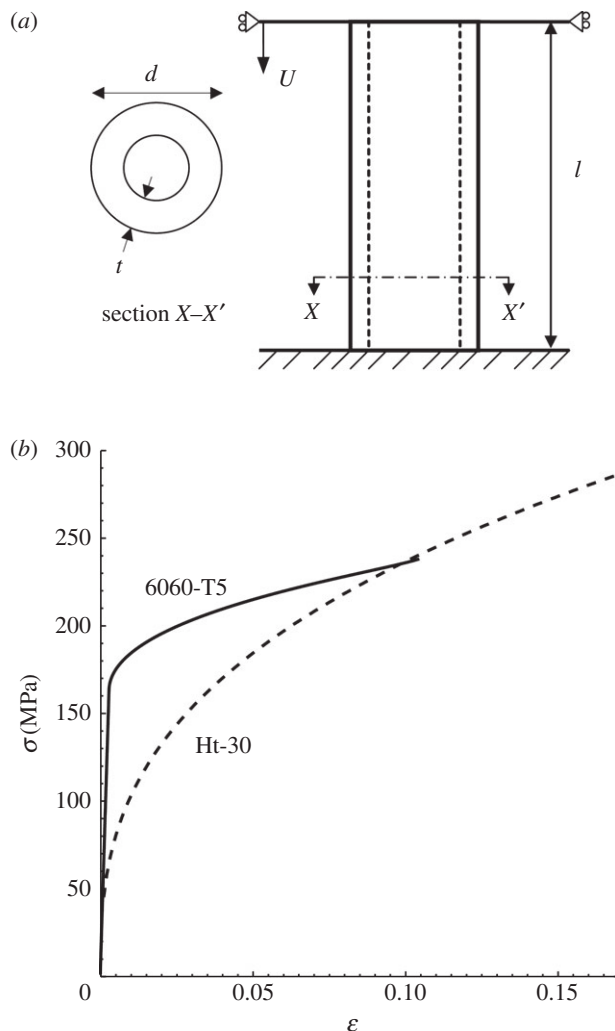


Figure 4. (a) A vertical cylindrical tube of circular cross section undergoing axial compression; (b) The true tensile stress versus logarithmic strain curves of the aluminium alloys used in constructing the collapse mechanism charts in figure 5.

(depending upon the particular specimen) and strain hardening comparable to that of the 6060-T6 aluminium alloy. Abramowicz & Jones identified the boundary in geometry space between global plastic buckling and progressive collapse by concertina-type modes. This boundary is included in figure 5b, and is in good agreement with that observed by Guillow *et al.* (2001) for the 6060-T5 aluminium alloy. This is consistent with the observation that the mild steel and 6060-T5 aluminium alloy have similar yield strains and similar work-hardening characteristics. Abramowicz & Jones (1997) also performed drop weight tests with an impact velocity on the order of 10 ms^{-1} . They observed that the range of geometries for which progressive folding occurs is greater for dynamic loading than for quasi-static loading. They also noted that the amount of energy absorbed

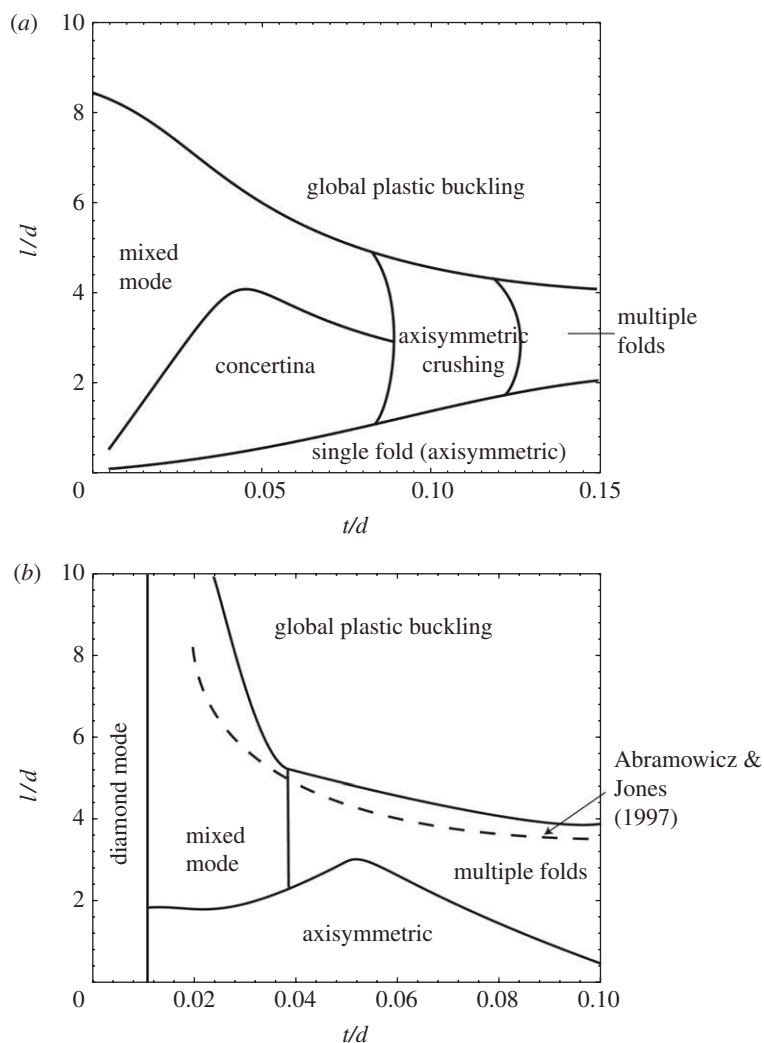


Figure 5. Collapse mechanism chart for circular vertical tubes made from (a) annealed aluminium Ht-30 (Andrews *et al.* 1983) and (b) 6060-T5 aluminium alloy (Guillow *et al.* 2001).

is much greater for progressive collapse than for global plastic buckling: materials and geometries which collapse by progressive folding are, therefore, preferred for energy absorption applications. The search for cellular material topologies that promote such responses is the motivation of this study.

(b) Scope of present study

Finite-element (FE) analysis is used to assess the compressive strength and energy absorption of sandwich cores with inclined and vertical tubes made from annealed AISI 304 stainless steel (a material with a low yield strain and high strain-hardening rate). A wide range of buckling modes is predicted for both the vertical and inclined tubes, and *collapse mechanism maps* are generated in order

to scope out the compressive response as a function of geometry. The analysis extends previous attempts to predict the mechanical properties of solid-section lattice cores using FE analysis by Hyun *et al.* (2003) and Côté *et al.* (2006): these previous studies were confined to a limited set of geometries and collapse modes for solid struts.

The analysis begins by examining the compressive axial collapse of ductile tubes of circular cross section (§2), in order to obtain the transverse compressive response of a sandwich plate with a core made from vertical tubes. The dependence of collapse mode upon tube geometry is investigated by FE analysis and is presented as a collapse mechanism map.

The geometry of a sandwich panel with a hollow pyramidal truss core is described in §3 along with the FE model used to analyse the collapse modes of the core under compressive loading. Attention is restricted to the through-thickness compression of a sandwich panel with rigid faces. Then, it suffices to consider the collapse response of a single representative inclined tube. In §4, a collapse mechanism map is constructed for the inclined tube; the map takes the core geometry as axes and displays the regimes of collapse mode. The peak compressive strength of the inclined tube is then used to determine the compressive strength of a sandwich panel with hollow pyramidal core; the relative density $\bar{\rho}$ of the core is expressed in terms of tube geometry. A *performance chart* for the hollow pyramidal core is thereby derived: it takes as axes the tube geometry, and displays contours of peak compressive strength depends and $\bar{\rho}$. The chart is used to obtain the optimal tube geometries that maximize compressive strength for any given $\bar{\rho}$. The study concludes with a discussion of the energy absorption capacity of the hollow pyramidal core, and with a comparison of the predicted collapse response with the measurements of Queheillalt & Wadley (submitted).

2. Finite-element predictions of the axial collapse of end-clamped tubes

A series of FE predictions are reported for the axial compressive response of circular cylindrical tubes of geometry defined in figure 4*a*. The wall material was treated as an elastic, plastic solid, with constitutive law given by conventional J2 flow theory. Isotropic hardening was assumed, and the uniaxial response was that for annealed AISI 304 stainless steel, as measured by Queheillalt & Wadley (submitted). The measured uniaxial tensile response of this steel is re-plotted in figure 6 in terms of the nominal compressive stress and strain behaviour.

The axial compressive response of end-clamped circular tube was modelled using the implicit version of the commercial FE software package, ABAQUS/Standard. Write d as outer diameter of the tube, l as its length and t as the wall thickness (figure 4*a*). The slenderness ratio l/d and thickness ratio t/d were varied over a wide range and the total number of geometries considered was on the order of 170. The tubes were modelled using continuum three-dimensional elements (hexahedral elements employing linear shape functions and reduced integration; C3D8R in ABAQUS notation). Typically, the three-dimensional elements were cubes with four or more elements across the thickness of the tube. The tubes were subjected to a progressively increasing axial displacement U between the ends of the tube (figure 4*a*). The ‘self contact’ option was used to prevent inter-penetration. A small initial imperfection was introduced into

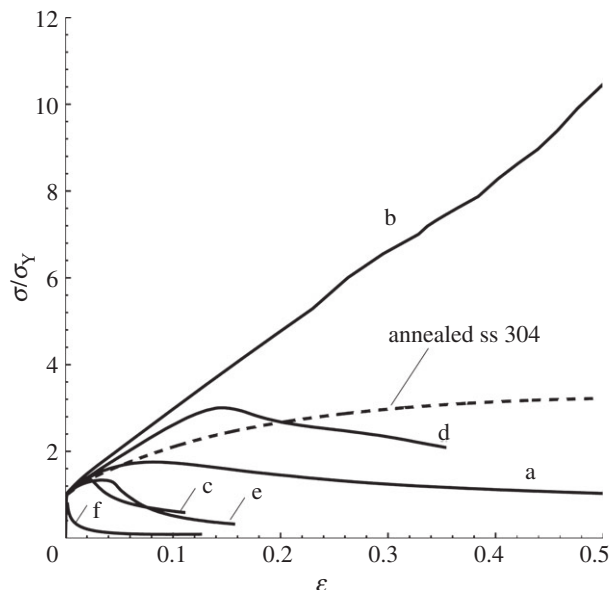





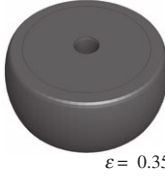








Figure 6. FE predictions of the compressive response of the six representative tube geometries. The response is plotted in terms of the normalized wall stress σ/σ_Y versus the applied nominal strain ε . The measured compressive nominal stress versus nominal strain response of annealed AISI 304 stainless steel is included; the yield strength is $\sigma_Y = 180$ MPa.

the FE model by superposition of the first four eigenmodes of elastic buckling. The maximum amplitude of each of the modes was equal, and the imperfection was introduced such that the maximum amplitude of the sum of the modes was $0.05t$. The analysis was performed using the finite strain option in ABAQUS (NLGEOM = YES in ABAQUS notation).

(a) Results

The predicted collapse modes in the post-buckled state were determined for the 170 geometries considered, and these are marked as discrete data points on a map of l/d versus t/d in the electronic supplementary material, figure A1 of appendix A. The collapse response was thereby catalogued into six distinct modes A–F, and the boundaries identified from the data points are available in the electronic supplementary material, figure A1; the data points have been included in the figure in order to give the degree of resolution of the operative modes. These modes are summarized in table 2, and the associated regimes of dominance are repeated in figure 7. Selected geometries (a–f) that collapse in each of the modes A–F, respectively, are marked on figure 7, and the collapse response for each selected geometry is plotted in figure 6 in terms of nominal average wall stress σ versus nominal compressive strain ε . (The wall stress σ is defined as the applied force divided by the initial tube wall cross-sectional area while the nominal axial strain ε is defined in terms of the axial shortening U and initial tube length l as $\varepsilon \equiv U/l$). In order to emphasize the degree of strain hardening prior to plastic buckling, the wall stresses in figure 6 have been

Table 2. Collapse modes of vertical tubes under compressive loading. Deformed geometries are shown at peak load and beyond peak load, with the nominal strain value ϵ reported. (Specimen (b) deforms by plastic barrelling and hence does not display a peak load.)

geometry	at peak load (exaggerated)	beyond peak load
(a) $\frac{t}{d} = 0.03,$ $\frac{l}{d} = 0.5$	 $\epsilon = 0.060$	 $\epsilon = 0.30$
(b) $\frac{t}{d} = 0.4,$ $\frac{l}{d} = 1$	 $\epsilon = 0.15$	 $\epsilon = 0.35$
(c) $\frac{t}{d} = 0.02,$ $\frac{l}{d} = 3$	 $\epsilon = 0.026$	 $\epsilon = 0.080$
(d) $\frac{t}{d} = 0.1,$ $\frac{l}{d} = 3$	 $\epsilon = 0.15$	 $\epsilon = 0.25$
(e) $\frac{t}{d} = 0.06,$ $\frac{l}{d} = 14.5$	 $\epsilon = 0.042$	 $\epsilon = 0.14$
(f) $\frac{t}{d} = 0.068,$ $\frac{l}{d} = 94$	 $\epsilon = 0.00085$	 $\epsilon = 0.01$

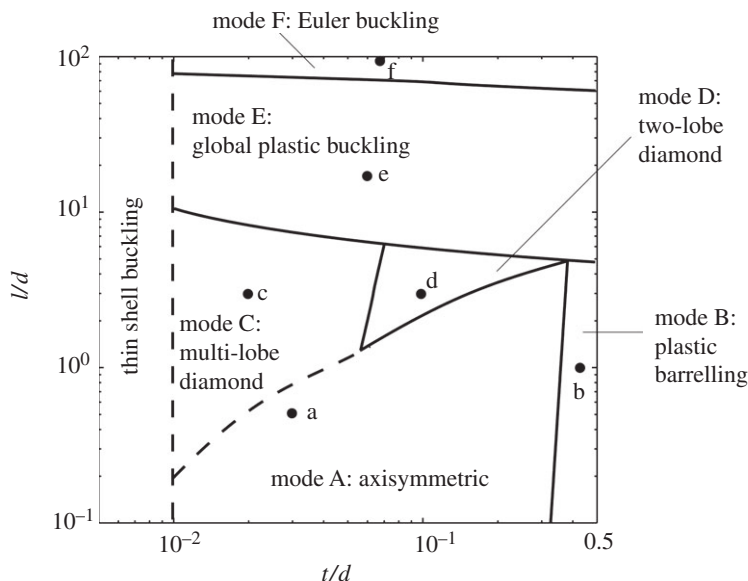


Figure 7. The predicted collapse mechanism map for vertical tubes. Note that the limiting geometry $t/d = 0.5$ corresponds to a solid vertical strut. The six representative geometries (a–f) are marked on the map.

normalized by the yield strength $\sigma_Y = 180$ MPa of the 304 stainless steel. Recall that the uniaxial compressive response of the annealed AISI type 304 stainless steel has been included in figure 6 as the reference case. The predictions shown in figure 6 are for a particular level of initial imperfection in tube geometry, as explained above. There is mild imperfection sensitivity and this is discussed in the electronic supplementary material, appendix A. Note that modes A and C–F display a peak, buckling load whereas mode B is plastic barrelling without bifurcation. We shall adopt the following convention for defining a peak load F_{pk} . For modes A and C–F, a peak load occurs at a nominal compressive strain of below 0.5, and we write this peak load as F_{pk} . Otherwise (i.e. for mode B), we write F_{pk} as the load at a nominal compressive strain of 0.5. The same convention will be adopted below for the inclined hollow tube.

For completeness, the deformed tubes (a–f) at peak load and beyond peak load are shown in table 2; the nominal axial strain of the deformed tubes, beyond peak load, is included. For geometries (a), (b) and (d–f), the collapse mode at peak load is the same as that deep in the post-buckled range. By contrast, geometry (c) displays axisymmetric folding at peak load, but this mode later bifurcates into a multi-lobe diamond mode (table 2). This switch in behaviour for geometries of type (c) leads to a modification to the collapse mechanism map associated with peak load: mode C is not present at peak load with mode A occupying that region. To illustrate this, the boundary between modes A and C is marked by a dashed line in figure 7. This transition in behaviour for tubes of geometry C was noted previously by Tvergaard (1983).

The collapse map of figure 7 has not been extended into the regime of thin-walled tubes ($t/d < 0.01$), as the buckling of thin tubes is highly imperfection sensitive, see, for example, Gerard & Becker (1957), Brush & Almroth (1975)

and Calladine (1995, 2001). In this regime, collapse is by plasticity-moderated elastic buckling and it proved problematic to obtain accurate FE results. Such thin-walled tubes are of limited practical interest for sandwich panel cores, and are excluded from the present study.

(b) *Discussion of the predicted collapse mechanisms*

The collapse mechanism map for tubes deep in the post-buckled state is shown in table 2 and in figure 7. It is more extensive than previous, experimentally obtained collapse charts (figure 5) as the elastic Euler buckling regime for slender tubes and the barrelling regimes for thick stubby tubes are included. It is emphasized that the predicted (and observed) collapse mode is somewhat sensitive to the initial imperfection for geometries that are near the boundaries of neighbouring collapse modes. Each collapse mode, deep in the post-buckled state, is now discussed in turn.

- *Mode A: Axisymmetric.* One or more axisymmetric bulges form along the length of the tube, with no switch in mode beyond peak load. Analytical models to give approximate expressions for this collapse mode have been developed for an ideally plastic solid by Alexander (1960) and Wierzbicki *et al.* (1992).
- *Mode B: Plastic barrelling.* Stubby thick-walled tubes do not buckle but rather deform in a barrelling mode. Barrelling is a consequence of the end constraint against radial expansion of the tubes. The response is continuously hardening with the applied loads higher than that required for uniaxial compression.
- *Mode C: Multi-lobe diamond.* An initial axisymmetric bulge is formed before peak load, but beyond peak load this mode bifurcates into a diamond pattern. Previously, this collapse mode for thin tubes has been observed experimentally by Horton *et al.* (1966) and theoretically by Yoshimura (1955), Pugsley & Macaulay (1960) and Tvergaard (1983).
- *Mode D: Two-lobe diamond.* The tube collapses by diamonds with two orthogonal lobes, as first observed by Andrews *et al.* (1983). This mode is observed at intermediate t/d and l/d (figure 7). Plastic constraint effects at the grips give rise to a response that is initially stiffer than the uniaxial material response, as evident from figure 6.
- *Mode E: Global plastic buckling.* The tube ovalizes and a plastic hinge is formed at mid-length. This results in significant softening in the structural response post-peak load.
- *Mode F: Euler buckling.* Slender tubes exhibit Euler elastic buckling. Beyond peak load, a plastic hinge developed at mid-span and the load drops sharply.

(c) *The dependence of peak force upon tube geometry*

The dependence of peak load F_{pk} upon tube geometry is summarized in figure 8 in which contours of normalized wall stress $\bar{F} = F_{\text{pk}}/(\sigma_Y A_0)$ are plotted in geometry space (l/d versus t/d), where $A_0 = \pi/4[d^2 - (d - 2t)^2]$ is the cross-sectional wall area of the tube (on a plane with unit normal along the tube axis).

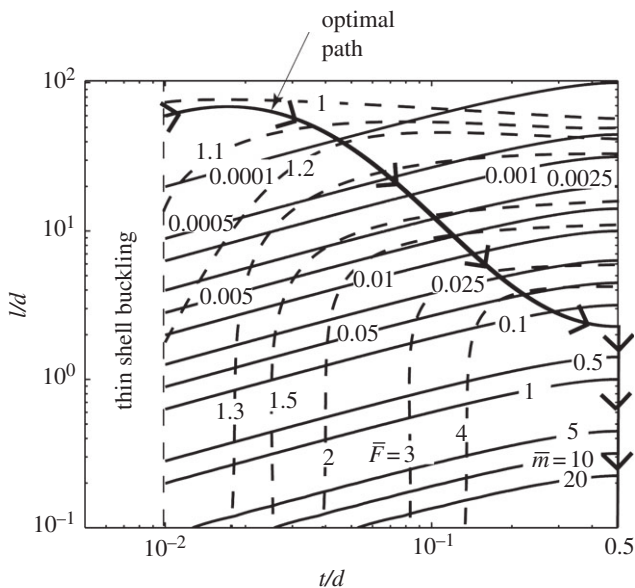


Figure 8. The normalized collapse strength \bar{F} and normalized mass \bar{m} of vertical tubes, plotted as a function of geometry (l/d and t/d). The trajectory of optimal geometries that maximize \bar{F} for any given \bar{m} is included.

For all geometries excluding the Euler buckling regime, peak load is attained beyond net section yield and the peak strength is enhanced by strain hardening. Additional plastic constraint occurs at the grips for thick-walled, stubby tubes.

The results plotted in figure 8 allow for a simple optimization to be performed on the choice of geometry of hollow tube that maximizes compressive strength. Suppose the task is to select the wall thickness t and outer diameter d of tube that maximize the peak compressive load F_{pk} , for a tube of given mass and given length. The mass of the tube is given by

$$m = \frac{\pi}{4} \rho l [d^2 - (d - 2t)^2], \quad (2.1)$$

in terms of the density ρ of wall material. Now introduce a reference mass m_r by considering a solid circular bar of length l and diameter $d = l$, such that

$$m_r = \frac{\pi}{4} \rho l^3, \quad (2.2)$$

and note that for a sandwich core of fixed height l , the reference mass m_r is constant. The mass of the tube can now be written in a dimensionless form as

$$\bar{m} = \frac{m}{m_r} = \left(\frac{d}{l}\right)^2 \left[1 - \left(1 - 2\frac{t}{d}\right)^2\right]. \quad (2.3)$$

Note that \bar{m} equals unity for a tube of vanishing inner diameter ($2t = d$) and of diameter $d = l$. For any fixed value of \bar{m} , a family of tube geometries ($t/d, l/d$) exists with equal mass and equal length l . Such contours of fixed normalized

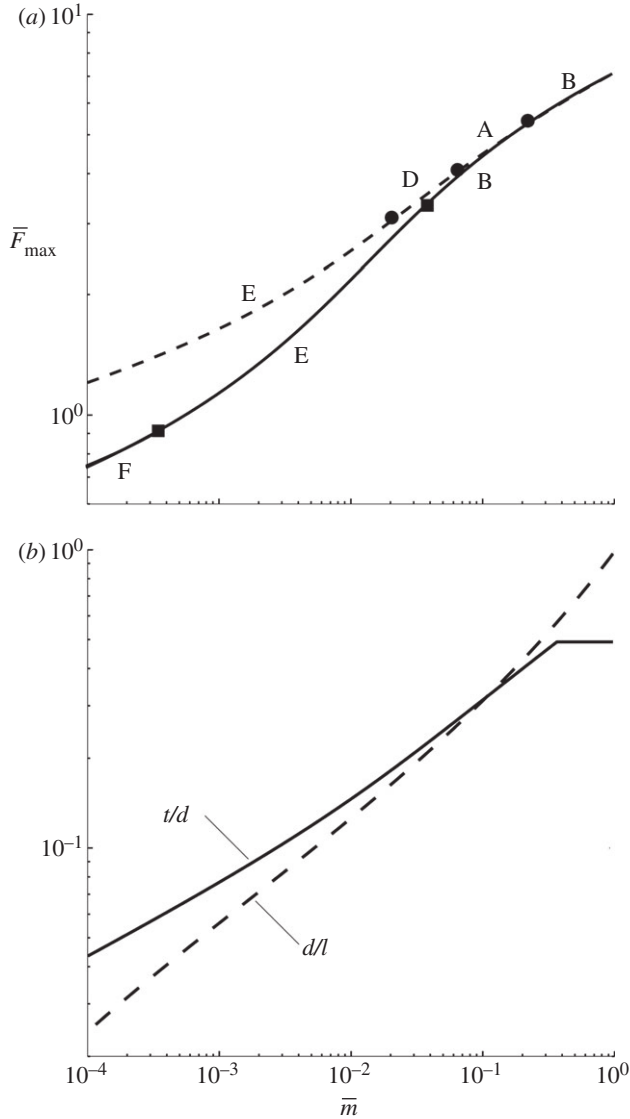


Figure 9. (a) The maximum normalized force \bar{F}_{\max} of the optimal vertical tubes as a function of normalized mass \bar{m} . The normalized collapse force for a solid column is included. The operative collapse modes range from E to B with increasing \bar{m} . (b) The optimal vertical tube geometry as a function of \bar{m} . Dashed lines, optimum tube; solid lines, solid column.

mass \bar{m} have been added to figure 8. Consider a trajectory of fixed \bar{m} and note that the collapse strength \bar{F} rises to a maximum (optimal value) and then drops again. Thus, an optimal geometry ($t/d, l/d$) exists for any given value of \bar{m} with a collapse load \bar{F}_{\max} . Upon performing this optimization procedure, a plot of optimal strength \bar{F}_{\max} and optimal geometry ($t/d, l/d$) can be generated as a function of \bar{m} (figure 9*a,b*). The optimal path is included in figure 8 and lies mainly in the collapse domain of global plastic buckling, mode E. The above

optimization procedure allows one to select the geometry (t, d) of vertical tubes for a sandwich core, when the height l of the core and the mass of each tube are prescribed.

The collapse strength of a solid circular bar ($2t = d$) is included in figure 9 for reference purposes; for the solid bar, the non-dimensional mass $\bar{m} = (d/l)^2$. We note that the collapse strength of the optimal tube is 1.5–2 times that of the bar of equal solid cross section, implying that there is significant structural advantage in the use of hollow tubes for a sandwich core. This is particularly true for $\bar{m} < 0.02$ with the advantage lost at higher values of $\bar{m} > 0.1$: at high \bar{m} , the deformation mode is plastic barrelling for both the tube and the solid strut. The operative collapse mode changes along the optimal path, with the regime of dominance from one mode to the next marked as data points on each optimal trajectory in figure 9a.

3. The pyramidal tube lattice

(a) Geometry

A unit cell of the hollow pyramidal lattice material, consisting of four inclined circular tubes, is shown in figure 3a. The geometry is defined in terms of the wall thickness t , outer tube diameter d , tube length l and inclination ω of each strut. The height of the core is $l \sin \omega$. In general, the tube centres can be offset by a distance of $2k$ as shown in figure 3b, with k constrained such that

$$k \geq k_{\min} = d \frac{\sqrt{1 + \sin^2 \omega}}{2 \sin \omega}. \quad (3.1)$$

The tubes touch each at the face sheets when $k = k_{\min}$. Unless otherwise specified, all results for the pyramidal core discussed subsequently assume that the tubes touch, $k = k_{\min}$. For arbitrary k , the relative density of the lattice is

$$\bar{\rho} = \frac{2\pi[d^2 - (d - 2t)^2]}{(4k + 2l \cos \omega)^2 \sin \omega}. \quad (3.2)$$

(b) Finite-element modelling of hollow tube pyramidal core

The FE method was again used to determine the compressive collapse response of a sandwich core comprising inclined tubes of circular cross section. The wall material was treated as an elastic, plastic solid, with constitutive law given by conventional J2 flow theory. Isotropic hardening was assumed, and the uniaxial response was again that for annealed AISI 304 stainless steel as described in §2.

It suffices to consider only a single tube of the pyramidal unit cell. The two face sheets of the sandwich panel were treated as rigid surfaces. It is assumed that the pyramidal core is perfectly bonded to the rigid faces and the end faces of each inclined tube approach each other by the compressive displacement U in the 3 direction of figure 3a. Note that there is no lateral motion in the 1 and 2 direction (figure 3a) and no end rotation. The representative tube is inclined at $\omega = 55^\circ$, as employed in the related experimental study by

Queheillalt & Wadley (submitted). Simulations¹ on thin-walled tubes with $t/d \leq 0.03$ were carried out using four-noded shell elements with reduced integration and based upon thick shell theory (S4R in the ABAQUS notation). Typically, there were 600 elements around the circumference. For thick-walled tubes ($t/d > 0.03$), the FE analysis was performed in a manner similar to that for the vertical tubes, recall §2*a*. Unlike the vertical tubes, no geometric imperfections were required for the inclined tube in order to induce buckling.

The vertical force P on each strut is along the 3 direction in figure 3 and is work conjugate to the applied vertical displacement U . The compressive nominal stress σ_n on the face sheets with a pyramidal core is given by

$$\sigma_n \equiv \frac{8P}{(4k + 2l \cos \omega)^2}, \quad (3.3)$$

while the corresponding nominal strain of the core of the sandwich plate is $\epsilon_n \equiv U/(l \sin \omega)$.

4. Collapse modes and performance charts for the pyramidal core

A collapse mechanism map has been constructed from the FE simulations, in similar fashion to that described above for the vertical tube. The inclined tube geometries considered are marked as discrete data points on a collapse mechanism map, shown in the electronic supplementary material, figure A3. The boundaries, without data points, are repeated in figure 10. Six distinct modes are identified. The geometries of inclined tubes representing these collapse modes (a–f) are displayed in table 3. The compressive responses are given in figure 11 in terms of the sandwich-core nominal stress $\sigma_n/(\bar{\rho}\sigma_Y)$ versus nominal strain ϵ_n . A variety of responses are observed ranging from rapid softening in mode F to a rapid strain-hardening response in mode B. Of the high aspect ratio truss responses, mode D exhibits the best energy-absorbing characteristics.

(a) *Buckled states*

Table 3 contains images of the deformed state of the six representative inclined tubes beyond peak load. These modes resemble those observed under axial compression (table 2) and so the same classification system is used as given in figure 7 and in table 2. The regimes of dominance for each of the six modes for the vertical tubes are included in figure 10 as dashed lines. Figure 10 clearly shows that the regimes of dominance of the various collapse modes are very similar for both the vertical and inclined tubes. The slight differences arise from the induced bending moment and reduced symmetry for the inclined tube. These considerations suggest that the collapse mechanism map of figure 10 is applicable to a wider range of strut inclinations than the assumed value of $\omega = 55^\circ$.

¹The FE simulations with three-dimensional elements took up to 30 h, those with shell elements took up to 20 h, running on an IBM x3550 with 2x Intel (R) Xeon (R) CPU E5345, single 2.33 GHz processor, 16 GB memory.

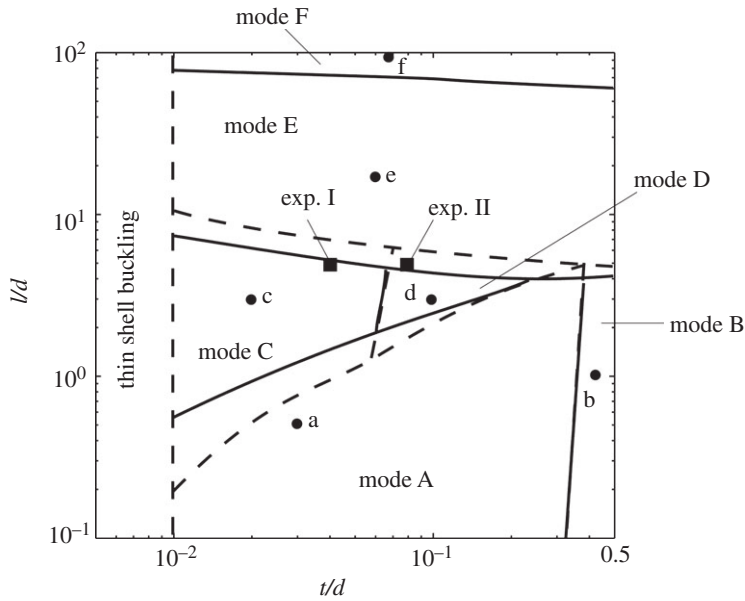


Figure 10. The collapse mechanism chart for inclined tubes. The six representative geometries (a–f) are shown, along with the two experimental (exp.) geometries, as considered by Queheillalt & Wadley (submitted). The dashed lines indicate the boundaries on the collapse mechanism map for vertical tubes (figure 7).

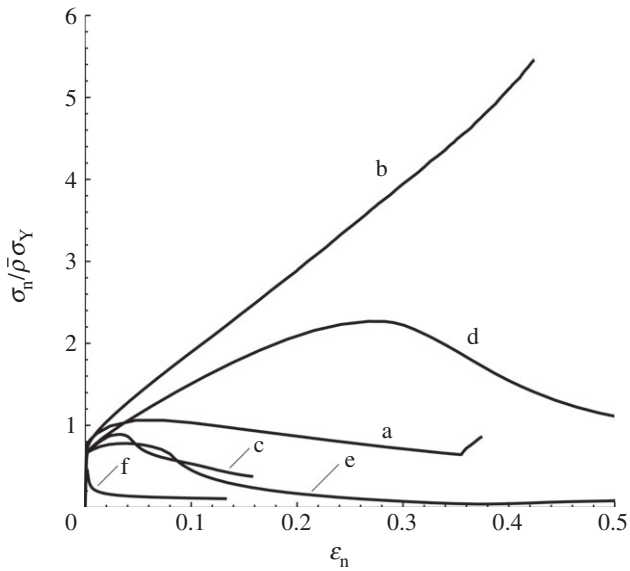

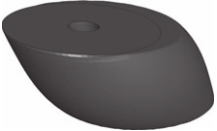

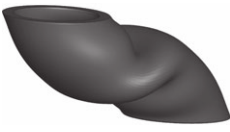




Figure 11. The compressive response of the six representative inclined tubes (a–f). The response is plotted in terms of the normalized nominal stress σ_n versus the applied nominal strain ϵ_n .

Table 3. Collapse modes of inclined tubes ($\omega = 55^\circ$) under compressive loading. Deformed geometries are shown beyond peak load, with the nominal strain value ϵ_n reported. (Specimen (b) deforms by plastic barrelling and hence does not display a peak load.)

mode name	post-peak load
(a) $\frac{t}{d} = 0.03,$ $\frac{l}{d} = 0.5$ $\bar{\rho} = 0.0644$	 $\epsilon_n = 0.15$
(b) $\frac{t}{d} = 0.4,$ $\frac{l}{d} = 1$ $\bar{\rho} = 0.4038$	 $\epsilon_n = 0.20$
(c) $\frac{t}{d} = 0.02,$ $\frac{l}{d} = 3$ $\bar{\rho} = 0.01384$	 $\epsilon_n = 0.08$
(d) $\frac{t}{d} = 0.1,$ $\frac{l}{d} = 3$ $\bar{\rho} = 0.06356$	 $\epsilon_n = 0.35$
(e) $\frac{t}{d} = 0.06,$ $\frac{l}{d} = 14.5$ $\bar{\rho} = 0.00442$	 $\epsilon_n = 0.10$
(f) $\frac{t}{d} = 0.068,$ $\frac{l}{d} = 94$ $\bar{\rho} = 0.000541$	 $\epsilon_n = 0.00080$

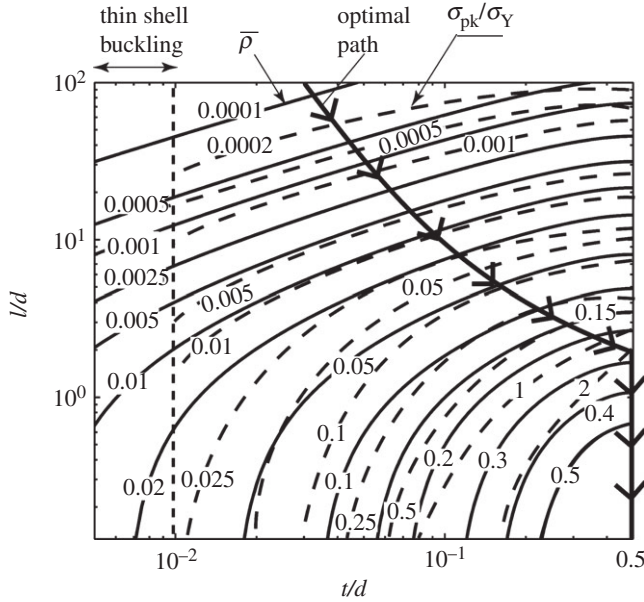


Figure 12. The normalized collapse strength σ_{pk}/σ_Y and relative density $\bar{\rho}$ of a hollow pyramidal core, plotted as a function of tube geometry (l/d and t/d). The trajectory of optimal geometries that maximize σ_{pk}/σ_Y at any $\bar{\rho}$ is included.

(b) Optimization of the pyramidal core

Figure 12 shows the performance chart for the hollow pyramidal lattice material under compressive loading: contours of normalized strength σ_{pk}/σ_Y are plotted on a chart with axes of l/d and t/d . Here, σ_{pk} is the peak value of σ_n . Contours of relative density of the pyramidal core (equation 5) are included in figure 12. Consider a trajectory of fixed $\bar{\rho}$ and note that σ_{pk} rises to a maximum value (which is the optimal value and denoted by σ_{max}) and then drops again. Thus, an optimal geometry exists for any given value of $\bar{\rho}$ that maximizes the peak strength. Similar to the vertical tubes, an optimization can be performed giving an optimal path in figure 12.

The results of the above optimization procedure are replotted in figure 13: the dependence of σ_{max} upon $\bar{\rho}$ is displayed in figure 13a, along with the associated optimal geometry t/d and d/l as a function of $\bar{\rho}$ in figure 13b. The peak strength of solid circular bars ($t/d = 0.5$) is also cross-plotted from figure 12 and is included in figure 13a. Over the range $10^{-3} \leq \bar{\rho} \leq 0.1$, the optimum core made from tubes has a higher strength than the solid strut core by a factor of about two. The advantage of tubes is the greatest for $\bar{\rho} \leq 0.002$ when the solid struts collapse by elastic Euler buckling. In contrast, at high values of $\bar{\rho}$, plastic barrelling (mode B) occurs for both the solid struts and tubes and hence any advantage of using tubes is lost. In order to assess the degree to which the strength of the inclined tube and solid strut compares with that of an ideal sandwich core made from a rigid, ideally plastic porous solid of relative density $\bar{\rho}$ and of parent material yield strength σ_Y , the peak strength σ_{max} in figure 13a has been normalized by

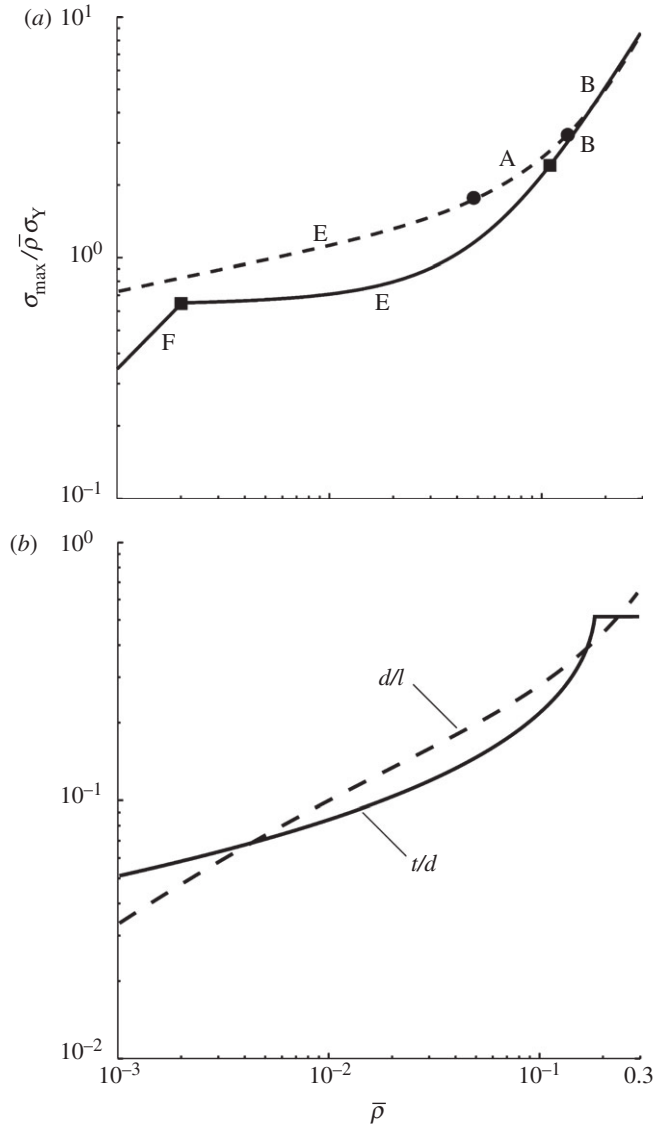


Figure 13. (a) The maximum collapse strength σ_{\max} of the optimal hollow pyramidal core as a function of $\bar{\rho}$. The normalized collapse strength for solid struts is included. The operative collapse modes range from E to B with increasing $\bar{\rho}$. (b) The optimum inclined tube geometry as a function of $\bar{\rho}$. Dashed lines, optimum tube; solid lines, solid inclined strut.

the factor $\bar{\rho}\sigma_Y$. It is evident from figure 13a that both the inclined tubes and solid struts are highly efficient structures, with compressive strengths exceeding the value of $\bar{\rho}\sigma_Y$ provided the relative density of the core is sufficiently high: to be precise, $(\sigma_{\max}/\sigma_Y\bar{\rho}) > 1$ when $\bar{\rho} > 0.005$ for the inclined hollow tube, and $(\sigma_{\max}/\sigma_Y\bar{\rho}) > 1$ when $\bar{\rho} > 0.035$ for the inclined solid strut. We emphasize that a value of $(\sigma_{\max}/\sigma_Y\bar{\rho})$ exceeding unity implies that buckling occurs deep in the plastic range after significant strain hardening has occurred.

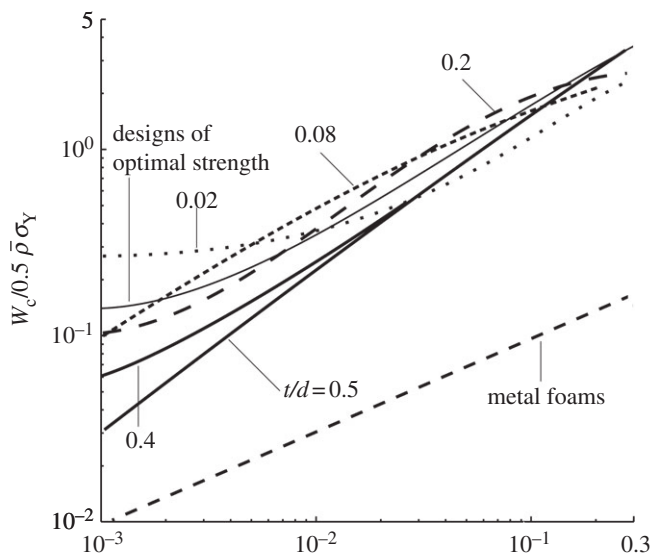


Figure 14. The normalized energy absorption per unit volume of the pyramidal core as a function of $\bar{\rho}$. Curves are shown for selected values of t/d ranging from 0.02 to the limiting case of a solid strut with $t/d = 0.5$. The energy absorption of the optimal pyramidal core is included.

(c) Energy absorption

A successful core of sandwich panel will be able to absorb a significant amount of energy in addition to having a high strength while also maintaining a large face sheet separation. Some collapse modes, such as elastic Euler buckling, are catastrophic in nature and absorb little energy. Thus, energy absorption is an important design metric in addition to compressive strength. We proceed to evaluate the energy absorption of the hollow pyramidal core as a function of geometry.

The compressive energy absorption capacity up to a practical nominal compressive strain of 0.5 is

$$W_c = \int_0^{0.5} \sigma_n d\varepsilon_n. \quad (4.1)$$

We proceed to present predictions for W_c normalized by the factor $0.5\bar{\rho}\sigma_Y$, which is the energy absorbed by an ideally plastic cellular solid of relative density $\bar{\rho}$ up to nominal strain of 0.5. Figure 14 shows the dependence of normalized energy absorption capacities upon lattice relative density $\bar{\rho}$. The pyramidal core made from solid inclined struts ($t/d = 0.5$) underperforms when compared with hollow pyramidal cores at low relative densities. By contrast, at high relative density, the tubes and solid struts undergo plastic barrelling and are comparable in energy absorption.

It is instructive to add to figure 14, the locus of absorbed energy for the optimal hollow trusses of geometry given in figure 13*b*. Although this lattice core is optimized from the perspective of peak strength it is *not* optimal in terms of absorbed energy especially at low values of $\bar{\rho}$.

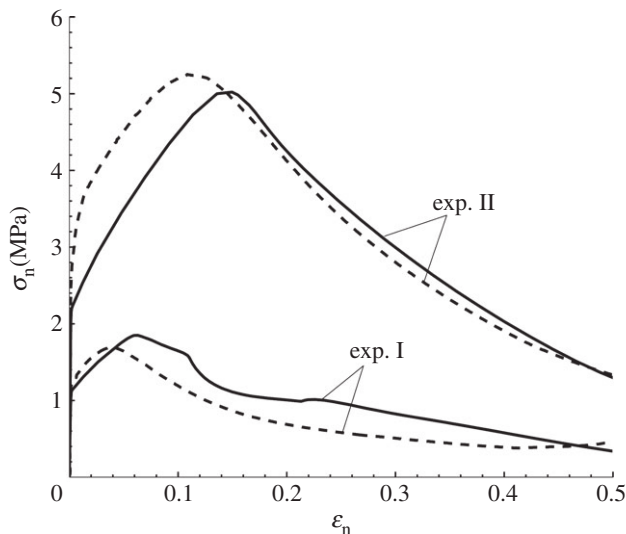


Figure 15. The measured and predicted compressive response of two hollow pyramidal cores, with tube geometries defined in figure 10. The experimental measurements have been taken from Queheillalt & Wadley (submitted). Solid lines, FE analysis; dashed lines, experiment.

The energy absorption capacity of metal foams up to a compressive strain of 0.5 is given as (Ashby *et al.* 2000)

$$W_c = 0.15\bar{\rho}^{3/2}\sigma_Y. \quad (4.2)$$

This prediction for the energy absorption of metal foams is included in figure 14. The metal foams absorb energy by collapsing at almost a constant stress value before densification. At high values of $\bar{\rho}$, the struts of the pyramidal core deform by plastic barrelling, and hence have a continuously hardening response with consequently high W_c . By contrast, at low values of $\bar{\rho}$, the struts of the pyramidal core collapse either by elastic or plastic buckling and the core has a strongly softening response. As a consequence, the gap between energy absorption capacity of the metal foams and that of the hollow pyramidal cores, is narrow at low $\bar{\rho}$.

(d) *Comparison of predicted and measured collapse responses of pyramidal core*

Queheillalt & Wadley (submitted) have performed a limited set of experiments on a hollow pyramidal core in order to measure the collapse response as a function of geometry. We now gauge the fidelity of the FE simulations by comparing our predictions with the observed response of two geometries as investigated by Queheillalt & Wadley (submitted). These geometries have the same value of l/d but different values of t/d , and are marked on the collapse mechanism map in figure 10: the geometry labelled exp. I lies at the boundary between modes C and E while the geometry labelled exp. II lies at the boundary between modes D and E. In the experiments, the pyramidal cores were constructed such that the tube centres were offset at the face sheets: the tubes do not touch their neighbours. The adopted spacing k , as defined in figure 3b, was $k = \sqrt{2}d$ and exceeds k_{\min} .

A comparison between the measured nominal compressive stress versus strain responses and the corresponding FE predictions is given in figure 15. Also, the observed and predicted deformation modes at an applied compressive strain of $\varepsilon_n = 0.5$ are included in table 1. Excellent agreement is noted between observations and predictions both for the collapse response and for the observed collapse mode, confirming the fidelity of the FE model for the hollow pyramidal core.

5. Concluding remarks

Numerical simulations have been performed to predict the compressive response of vertical and inclined tubes made from annealed stainless steel 304. First, a collapse mechanism classification map, with axes l/d and t/d , is presented for vertical tubes. Six distinct collapse modes are identified ranging from elastic Euler buckling of slender tubes to plastic barrelling of stubby thick-walled tubes.

Next, a pyramidal lattice core whose unit cell comprises four inclined tubes is analysed. The predicted collapse modes for the inclined tubes are similar to the vertical tubes with some minor differences owing to the induced bending moment in the inclined tubes. In similar manner to that achieved for the vertical tubes, performance charts are constructed to quantify sandwich-core strength as a function of its relative density. Also, the ideal tube geometry ($t/d, l/d$) that maximizes the compressive strength is identified as a function of relative density. For both the vertical and inclined tubes, we find that the optimized tubes outperform their solid equivalents at low densities; however, this advantage is lost at higher densities when plastic barrelling becomes the dominant deformation mode.

The FE predictions are in excellent agreement with a limited set of measurements on the compression of a pyramidal core made from hollow struts, as reported by Queheillalt & Wadley (submitted). Our study focused on a stainless steel of high strain-hardening capacity, and upon a pyramidal core of strut inclination $\omega = 55^\circ$ in order to make contact with the experimental study of Queheillalt & Wadley (submitted). The material strain hardening and strut inclination are design variables and their significance should be addressed in future studies.

The above analysis of the inclined tube applies to the collapse of a wide range of sandwich panel cores, and is not limited to the pyramidal core. For example, the response can be deduced for a hollow tetragonal core and for a pentagonal arrangement of core struts. Indeed, the analysis can be extended to randomly arranged inclined tubes as a sandwich core, provided the face sheets are rigid and are constrained to approach each other with zero relative sliding.

The authors are grateful for financial support from the EPSRC contract EP/D055806/1 and from the Office of Naval Research under ONR contract N00014-07-10114 (Dr D. Shifler, Programme Manager).

References

- Abramowicz, W. & Jones, N. 1997. Transition from initial global bending to progressive buckling of tubes loaded statically and dynamically. *Int. J. Impact Eng.* **19**, 415–437. (doi:10.1016/S0734-743X(96)00052-8)

- Alexander, J. M. 1960 An approximate analysis of the collapse of thin cylindrical shells under axial loading. *Q. J. Mech. Appl. Math.* **13**, 10–15. (doi:10.1093/qjmam/13.1.10)
- Andrews, K. R. F., England, G. L. & Ghani, E. 1983 Classification of the axial collapse of cylindrical tubes under quasi-static loading. *Int. J. Mech. Sci.* **25**, 687–696. (doi:10.1016/0020-7403(83)90076-0)
- Ashby, M. F., Evans, A. G., Fleck, N. A., Gibson, G. J., Hutchinson, J. W. & Wadley, H. N. G. 2000 *Metal foams: a design guide*. Oxford, UK: Butterworth Heinemann.
- Brush, D. O. & Almroth, B. O. 1975 *Buckling of bars, plates and shells*. New York, NY: McGraw-Hill Book Co.
- Calladine, C. 1995 Understanding imperfection-sensitivity in the buckling of thin-walled structures. *Thin-walled Struct.* **23**, 215–235. (doi:10.1016/0263-8231(95)00013-4)
- Calladine, C. R. 2001 A shell buckling paradox resolved. In *Advances in the mechanics of plates and shells* (eds D. Durban, D. Givoli & J. Simmonds), pp. 119–135. Dordrecht, The Netherlands: Kluwer Academic Publishers.
- Côté, F., Deshpande, V. S., Fleck, N. A. & Evans, A. G. 2006 The compressive and shear responses of corrugated and diamond lattice materials. *Int. J. Solids Struct.* **43**, 6220–6242. (doi:10.1016/j.ijsolstr.2005.07.045)
- Deshpande, V. S. & Fleck, N. A. 2001 Collapse of truss core sandwich beams in 3-point bending. *Int. J. Solids Struct.* **38**, 6275–6305. (doi:10.1016/S0020-7683(01)00103-2)
- Deshpande, V. S., Fleck, N. A. & Ashby, M. F. 2001a Effective properties of the octet-truss lattice material. *J. Mech. Phys. Solids* **49**, 1747–1769. (doi:10.1016/S0022-5096(01)00010-2)
- Deshpande, V. S., Fleck, N. A. & Ashby, M. F. 2001b Foam topology: bending versus stretching dominated architectures. *Acta Materialia* **6**, 1035–1040. (doi:10.1016/S1359-6454(00)00379-7)
- Evans, A. G., Hutchinson, J. W. & Ashby, M. F. 1998 Cellular metals. *Curr. Opin. Solid State Mater. Sci.* **3**, 288–303. (doi:10.1016/S1359-0286(98)80105-8)
- Evans, A. G., Hutchinson, J. W., Fleck, N. A., Ashby, M. F. & Wadley, H. N. G. 2001 The topological design of multifunctional cellular metals. *Prog. Mater. Sci.* **46**, 309–327. (doi:10.1016/S0079-6425(00)00016-5)
- Fleck, N. A. & Deshpande, V. S. 2004 The resistance of clamped sandwich beams to shock loading. *J. Appl. Mech.* **71**, 386–401. (doi:10.1115/1.1629109)
- Gerard, G. & Becker, H. 1957 Handbook of structural stability part III: buckling of curved plates and shells. Technical note, 3783, NACA, Washington, DC.
- Guillow, S. R., Lu, G. & Grzebieta, R. H. 2001 Quasi-static axial compression of thin-walled circular aluminium tubes. *Int. J. Mech. Sci.* **43**, 2103–2123. (doi:10.1016/S0020-7403(01)00031-5)
- Horton, H. G., Bailey, S. C. & Edwards, A. M. 1966 Nonsymmetric buckle patterns in progressive plastic buckling. *Exp. Mech.* **6**, 433–444. (doi:10.1007/BF02326556)
- Hyun, S., Karlsson, A. M., Torquato, S. K. & Evans, A. G. 2003 Simulated properties of Kagome and tetragonal cores. *Int. J. Solids Struct.* **40**, 6989–6998. (doi:10.1016/S0020-7683(03)00350-0)
- Johnson, W. & Reid, S. R. 1978 Metallic energy dissipating systems. *Appl. Mech. Rev.* **31**, 277–288.
- Kooistra, G. W. & Wadley, H. N. G. 2007 Lattice truss structures from expanded metal sheet. *Mater. Design* **28**, 507–514. (doi:10.1016/j.matdes.2005.08.013)
- Pugsley, A. & Macaulay, M. 1960 The large scale crumpling of thin cylindrical shells. *Q. J. Mech. Appl. Math.* **13**, 1–9. (doi:10.1093/qjmam/13.1.1)
- Queheillalt, D. T. & Wadley, H. N. G. 2005a Cellular metal lattices with hollow trusses. *Acta Materialia* **53**, 303–313. (doi:10.1016/j.actamat.2004.09.024)
- Queheillalt, D. T. & Wadley, H. N. G. 2005b Pyramidal lattice truss structures with hollow trusses. *Mater. Sci. Eng. A* **397**, 132–137. (doi:10.1016/j.msea.2005.02.048)
- Queheillalt, D. T. & Wadley, H. N. G. Submitted. Hollow pyramidal lattice truss structures. *Int. J. Mater. Res.*
- Queheillalt, D. T., Carbajal, G., Peterson, G. P. & Wadley, H. N. G. 2008 A multifunctional heat pipe sandwich panel structure. *Int. J. Heat Mass Transfer* **51**, 312–326. (doi:10.1016/j.ijheatmasstransfer.2007.03.051)

- Tian, J., Lu, T. J., Hodson, H. P., Queheillalt, D. T. & Wadley, H. N. G. 2006 Cross flow heat exchange of textile cellular metal core sandwich panels. *Int. J. Heat Mass Transfer* **50**, 2521–2536. (doi:10.1016/j.ijheatmasstransfer.2006.11.042)
- Timoshenko, S. P. & Gere, J. M. 1961 *Theory of elastic stability*. New York, NY: McGraw-Hill.
- Tvergaard, V. 1983 On the transition from a diamond mode to an axisymmetric mode of collapse in cylindrical shells. *Int. J. Solids Struct.* **19**, 845–856. (doi:10.1016/0020-7683(83)90041-0)
- Wadley, H. N. G. 2006 Multifunctional periodic cellular metals. *Phil. Trans. R. Soc. A* **364**, 31–68. (doi:10.1098/rsta.2005.1697)
- Wicks, N. & Hutchinson, J. W. 2001 Optimal truss plates. *Int. J. Solids Struct.* **38**, 5165–5183. (doi:10.1016/S0020-7683(00)00315-2)
- Wierzbicki, T., Bhat, S. U. & Abramowicz, W. 1992 Alexander revisited: a two folding elements model of progressive crushing tubes. *Int. J. Solids Struct.* **29**, 3269–3288. (doi:10.1016/0020-7683(92)90040-Z)
- Yoshimura, Y. 1955 On the mechanism of buckling of a circular cylindrical shell under axial compression. NACA Technical Memorandum 1390 (accession ID: 93R23165).
- Zenkert, D. 1995 *An introduction to sandwich construction*. Sheffield, UK: Engineering Materials Advisory Service.